

EFDA–JET–CP(01)08-03

D.Testa, A.Fasoli, D.N.Borba, A.Jaun and S.E.Sharapov
and JET EFDA Contributors

Experimental Studies of Alfvén Modes Stability on the JET Tokamak

Experimental Studies of Alfvén Modes Stability on the JET Tokamak

D.Testa¹, A.Fasoli¹, D.N.Borba^{2,3}, A.Jaun⁴ and S.E.Sharapov⁵
and JET EFDA Contributors

EURATOM-UKAEA Fusion Association, Culham Science Centre, Abingdon, OX14 4XB, United Kingdom.

¹*Plasma Science and Fusion Center, Massachusetts Institute of Technology, Cambridge, USA*

²*Associação EURATOM/IST, Av. Rovisco Pais, 1049-001 Lisboa, Portugal*

³*EDFA Close Support Unit, Culham Science Center, Abingdon OX14 3DB UK*

⁴*Euratom - Alfvén Laboratory, Teknikringen 31, KTH, SE-100 44 Stockholm, Sweden*

⁵*Euratom— UKAEA Fusion Association, Culham Science Center, Abingdon, OX14 3DB, UK*

**See Annex of J. Pamela et al., “Overview of Recent JET Results and Future Perspectives”, Fusion Energy 2000 (Proc. 18th Int. Conf. Sorrento, 2000), IAEA, Vienna (2001).*

Preprint of Paper to be submitted for publication in Proceedings of the
7th IAEA TCM on Energetic Particles,
(Gothenburg, 8-11 October 2001)

“This document is intended for publication in the open literature. It is made available on the understanding that it may not be further circulated and extracts or references may not be published prior to publication of the original when applicable, or without the consent of the Publications Officer, EFDA, Culham Science Centre, Abingdon, Oxon, OX14 3DB, UK.”

“Enquiries about Copyright and reproduction should be addressed to the Publications Officer, EFDA, Culham Science Centre, Abingdon, Oxon, OX14 3DB, UK.”

INTRODUCTION

The linear stability properties of Alfvén modes are studied on JET using an active excitation technique [1,2]. The Saddle Coils drive low amplitude, $|\delta B/B| \approx 10^{-6}$, stable plasma modes with toroidal mode number $n=0 \div 2$. The diagnostic technique uses repetitive sweeps of the driving frequency in a pre-defined range, controlled in real-time. The plasma response is extracted from background noise using synchronous detection, and is used to identify in real-time the resonance corresponding to a global mode. When a resonance is found, the real-time controller locks to that frequency and tracks the mode. This provides a direct evaluation of the mode damping rate, γ/ω from the width of the frequency sweep. Two systems are used to measure fast fluctuation data. The KC1F system [3] is a 8-channel, $1\text{MHz}/4\text{s}$ continuous digitizer used to analyze magnetic and reflectometry data in the frequency range $5 \leq f(\text{kHz}) \leq 500$. This system is particularly suitable to follow the time evolution of the instability. The CATS system [4] collects and digitizes a large number of channels generally using short time snapshots. This system is useful to determine the position of the instability using the cross-correlation between the magnetic and other radially localized measurements, such as soft X-rays, reflectometry or electron cyclotron emission.

1. LINEAR STABILITY PROPERTY OF ALFVÉN EIGENMODES.

New data have been obtained on the dependence of the damping rate of radially extended $n=0$ Global Alfvén Eigenmodes (GAEs) and $n=1 \div 2$ Toroidal Alfvén Eigenmodes (TAEs) on the elongation and triangularity, the plasma beta, the normalized Larmor radius, and the λ -parameter used in the so-called radiative damping model [5]. These experiments were performed in the conventional tokamak scenario with a monotonic q-profile ($q_0 \approx 1$), with the aim of discriminating between the different models for the AE damping mechanisms, to provide accurate extrapolation for future burning fusion plasma experiments.

Figure 1 shows the damping rate of $n=0$ and $n=1$ AEs as a function of the triangularity averaged above and below the midplane, $\langle \delta \rangle = (\delta_{\text{UP}} + \delta_{\text{LOW}})/2$, and $\kappa(r/a=0.5) = \kappa_0 + (\kappa_{95} - \kappa_0)(r/a)^2/(0.95)^2$, the elongation at mid radius [6]. The γ/ω for these low-n AEs strongly increases with δ and κ . This effectively gives the possibility of developing real-time tools to simulate and control the stability of AEs being driven unstable by fusion-born alpha particles.

The measured γ/ω for a $n=1$ TAE is shown in Fig.2 for a discharge where P_{NBI} was ramped-up to study the effect of T_i and β . It is found that the increase in β splits the frequency spectrum, up to $P_{\text{NBI}} \approx 5\text{MW}$, contributing to reduce γ/ω . Figure 3 shows an example of frequency splitting during the NBI phase, for $P_{\text{NBI}} = 0 \rightarrow 3\text{MW}$. For $P_{\text{NBI}} > 2\text{MW}$, two other modes are measured during the same frequency scan, $54 < t(\text{s}) < 55$, with $\gamma/\omega < 0.5\%$. This result is consistent with the prediction of splitting of a single TAE into multiple kinetic AEs [7].

The radiative damping model [5] predicts a clear dependence of the TAE damping rate on the ion Larmor radius ρ^* and the λ -parameter, $\lambda = 4(m\sigma\rho^*/r_m) \varepsilon_m^{3/2} (3/4 + T_e/T_i)^{1/2}$, $(\gamma/\omega)_{\text{RAD}} \propto \exp(-\sigma^2/\lambda)$. Here r_m is the position of the m/n TAE, $\varepsilon_m = 2R/5r_m$, and all plasma parameters are

averaged in the gap region $\Delta = rm(1 \pm \bullet m/m)$. Figure 4 shows the variation of γ/ω for the $m/n=2/1$ TAE as a function of ρ^* and λ for a series of discharges characterized by a weak core magnetic shear $\sigma_0 \approx 0.1$. Here the magnetic field and plasma current were ramped at fixed $q0 \approx 0.8$ and $q_{95} \approx 2.8 \div 2.9$, to change ρ^* , and hence λ . The experiment clearly shows that $(\gamma/\omega)_{MEAS} \approx 10 \times (\gamma/\omega)_{RAD}$, and $(\gamma/\omega)_{RAD}$ predicts a different scaling for increasing ρ^* and λ . These results suggest that the radiative damping model may not be sufficient to predict correctly the TAE stability limit in burning plasma experiments.

2. NON-LINEAR WAVE-PARTICLE PHYSICS.

A new class of instabilities in the Alfvén frequency range, excited by ICRF-driven fast ions, is observed during the current ramp-up phase of JET Optimized Shear (OS) plasmas with a nonmonotonic q-profile. Figure 5 shows a typical example of such measurements.

These $n=1-7$ Alfvénic modes observed in OS plasmas with non-monotonic q-profile do not follow the scaling $f(t) \propto B/q \sqrt{n_i + nf \phi_{TOR}}$ typical of the ICRF-driven TAEs which appear in a plasma with monotonic q-profile. The modes originate in the Alfvén continuum around $r/a \approx 0.2$ at $f \approx 20 \div 50 kHz$, eventually merging after $\approx 100 \div 400 ms$ into a TAE at $f \approx f_{TAE}(qMIN)$ around $r/a = r/a(qMIN) \approx 0.5$. The chirping rate is proportional to the toroidal mode number, $df/dt \bullet n$, and is independent on m . These modes have been recently interpreted as a variety of Global Alfvén Modes (GAE) [8] that exist near the local maximum of the Alfvén continuum at a q-minimum surface [9].

These modes have also been recently identified [10] as resonantly excited EPMs [11] and not as a TAEs due to the strength of the growth rate, which is comparable with the gap width. Non-linear simulations, using a 3D hybrid MHD-GK code [12], demonstrate strong resonant excitations of an EPM around $r/a=0.2$, in agreement with the measurements, where the fast ion resonant drive is maximized. The mode structure evolves as the source is radially displaced and weakened. The mode then merges into an Alfvén mode near the TAE gap at the position of the q-minimum surface at $r/a \approx 0.5$. This rapid nonlinear evolution occurs on a time scale of $\approx 100 \tau_A$ and explains why experimental observations of mode frequencies fit well with those of shear Alfvén waves localized near the q-minimum surface [9].

Pellet injection during steady-state ICRF-heated discharges provides a good example of the nonlinear behavior of fast ion driven AEs. The pellet injection produces a density perturbation on a time scale comparable to the Alfvén time, $(n/\Delta n) \Delta t \approx \tau_A$: over this period the resonance condition $\bullet A = \bullet ||$ sweeps a significant fraction of the fast ion distribution function. This phenomenon is expected to cause a radial redistribution of the fast ions. Figure 6 shows the TAE spectrum for two discharges with similar background plasma, respectively with pellet injection from the low and the high magnetic field side. In both cases the observed stabilization of TAEs suggests a reduction in the drive. The sawtooth-like event caused by the pellet injection can trigger EAEs by redistributing the fast particles from the core towards the more external region

where the EAE spectrum is localized. Thus the clear differences observed in the two pellet injection scenarios can be accounted for by a much smaller increase in the plasma density for outboard launched pellets, which in turn produces a weaker sawtooth-like crash.

SUMMARY AND CONCLUSIONS.

The linear stability of low- n AEs has been studied for the conventional tokamak scenario as a function of the plasma shape, ρ^* and β . The damping rate is very sensitive to the edge shaping (κ , δ), suggesting a real-time control mechanism for AEs approaching the marginal stability limit. The reduction in γ/ω and the frequency splitting observed for increasing β may be accounted for through excitation of kinetic AEs. The measured γ/ω is significantly larger than that predicted by the radiative damping model and shows an opposite scaling for increasing ρ^* and λ . Various classes of Alfvén instabilities have been observed and their analysis is providing detailed insights into non-linear wave-particle interaction mechanisms relevant for burning plasma experiments.

ACKNOWLEDGEMENTS

This work has been conducted under the European Fusion Development Agreement. D.Testa and A.Fasoli were partly supported by DoE contract No. DE-FG02-99ER54563.

REFERENCES

- [1] A.Fasoli et al., *Phys. Rev. Lett.* **75**, 645 (1995).
- [2] A.Fasoli et al., *Phys. Plasmas* **7**, 1816 (2000).
- [3] R.Heeter et al., *Rev Sci. Instrum.* **71**, 4092 (2000).
- [4] K.Blackler et al., *IEEE Trans. on Nucl. Science* **41**, 111 (1994).
- [5] G.Fu et al., *Phys Plasmas* **3**, 4036 (1996).
- [6] D.Testa and A.Fasoli, *Nucl. Fusion* **41**, 809 (2001).
- [7] A.Jaun et al., *Plasma Phys. Control. Fusion* **39**, 549 (1997).
- [8] J.Goedbloed, *Physica* **D12**, 107 (1984).
- [9] H.Berk et al., IFT Conference, Santa Fe, USA, 2001; and S.Sharapov et al., this Conference.
- [10] D.Testa et al., EPS Conference 2001, Madeira, Portugal.
- [11] L.Chen, *Phys. Plasmas* **1**, 1519 (1994);
- [12] S.Briguglio et al., *Phys. Plasmas* **2**, and this Conference.

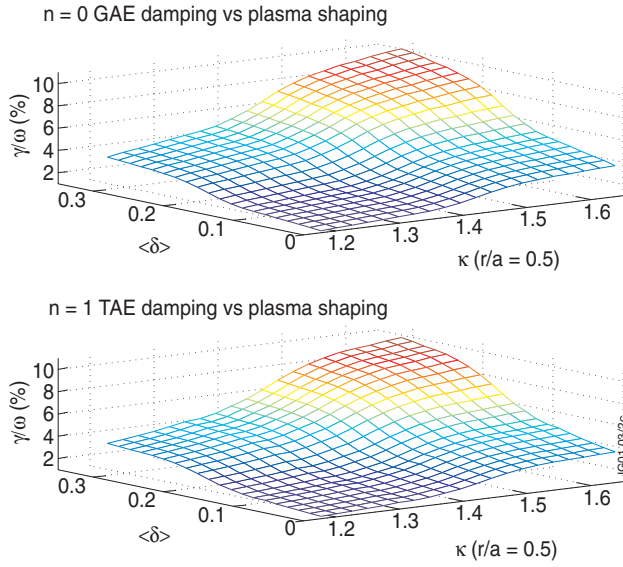


Figure.1: Limiter plasmas (pure ohmic heating) with: $B_{\phi 0}=2.2T, I_p=2.6MA, n_{e0} \approx 2.5 \times 10^{19}m^{-3}, \langle ne \rangle \approx 2 \times 10^{19}m^{-3}, T_{e0} \approx 2.5keV, \langle Te \rangle \approx 1keV, q_0 \approx 0.9, q_{95} \approx 4, \sigma_0 \approx 1.$

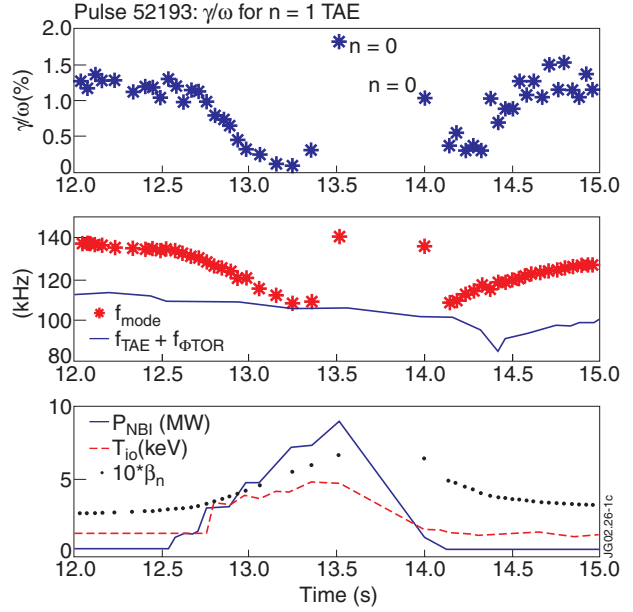


Figure.2: Limiter plasma with $B_{\phi 0}=2.6T, I_p=2.5MA, q_0 \approx 0.8, q_{95} \approx 3, \sigma_0 \approx 1, \sigma_{95} \approx 9.5, n_{e0} \approx 2 \div 4 \times 10^{19}m^{-3}, \kappa_0 \approx 1.2, \kappa_{95} \approx 1.4, \delta_{UP} \approx 0.06 \approx \delta_{LOW}, T_{e0} \approx 2 \div 4keV, T_{i0} \approx 1 \div 5keV.$

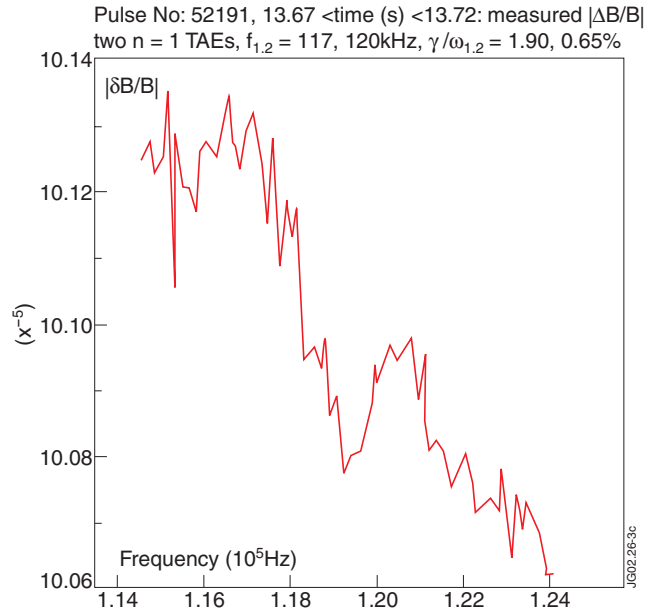
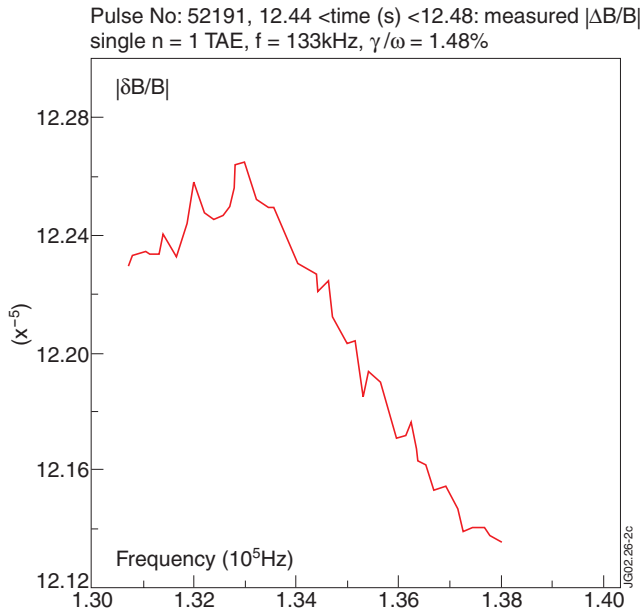


Figure.3: Left: ohmic phase, Right: PNBI=3MW. During this phase the plasma parameters are $B_{\phi 0}=2.6T, I_p=2.5MA, q_0 \approx 0.8, q_{95} \approx 3.2, \sigma_0 \approx 1, \sigma_{95} \approx 10, \kappa_0 \approx 1.2, \kappa_{95} \approx 1.4, \delta_{UP} \approx 0.07 \approx \delta_{LOW}, n_{e0} \approx 2.2 \rightarrow 3.2 \cdot 10^{19}m^{-3}, T_{i0} \approx 1.5keV, T_{e0} \approx 3keV.$

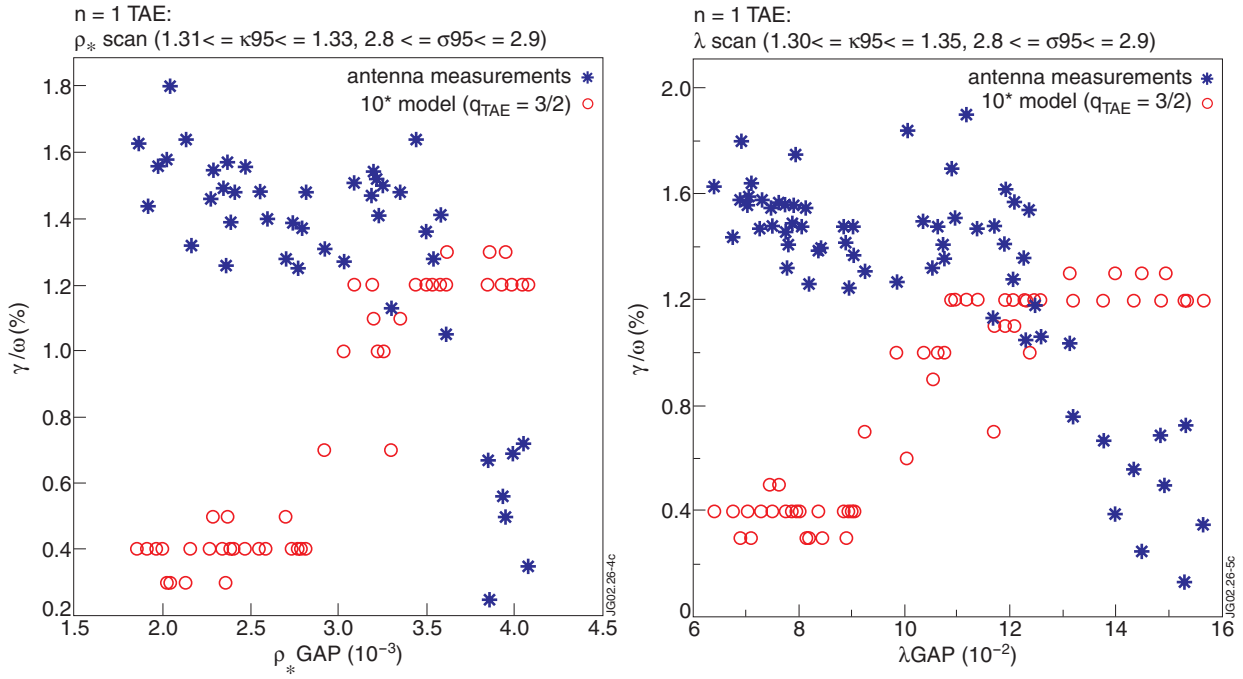


Figure.4: Plasma in limiter configuration with $n_{e0} \approx (1.8 \pm 3) \times 10^{19} m^{-3}$, $T_{e0} \approx (0.8 \pm 2.6) keV$, $T_{i0} \approx (0.6 \pm 2.3) keV$, $\delta \approx 0.05$.

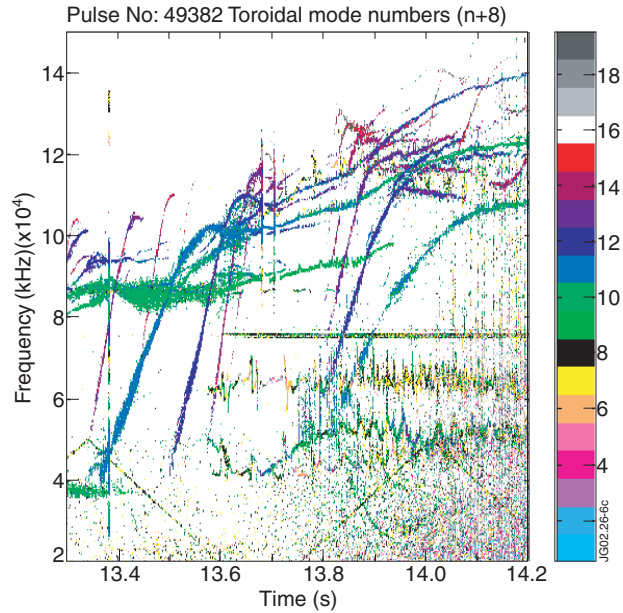


Figure.5: Magnetic spectrum in the preheating phase of an OS plasma with non-monotonic q -profile.

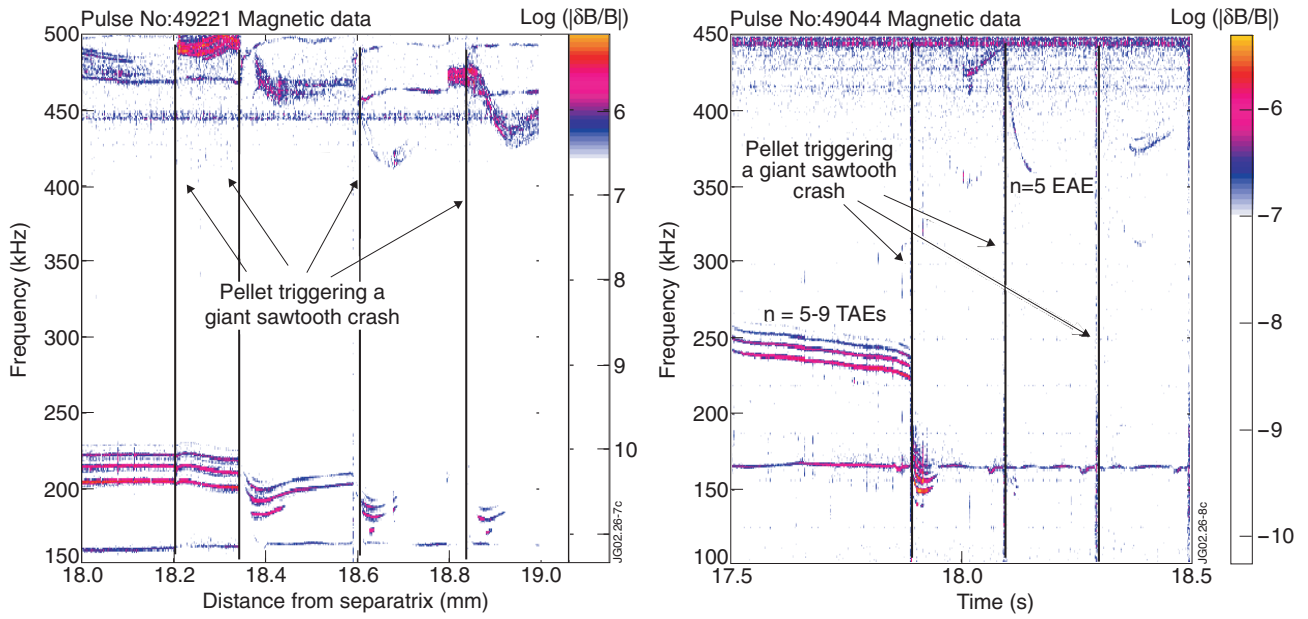


Figure.6: Left: low-field side pellet injection for #49221; Right: high-field side pellet injection for #49044. For both discharges $n_e > 4 \times 10^{19} \text{m}^{-3}$, $T_e \approx T_i \approx 2.5 \text{keV}$, $q_0 \approx 1$, $B_{\phi 0} = 3.2 \text{T}$, $I_p = 2.5 \text{MA}$, $P_{ICRF} = 7.5 \text{MW}$ and $P_{NBI} = 1 \text{MW}$.